Ab initio global potential, dipole, adiabatic, and relativistic correction surfaces for the HCN–HNC system

Tanja van Mourik, Gregory J. Harris, Oleg L. Polyansky, Jonathan Tennyson, Attila G. Császár, and Peter J. Knowles

---

Articles you may be interested in

Ab initio study of the RbSr electronic structure: Potential energy curves, transition dipole moments, and permanent electric dipole moments
J. Chem. Phys. 141, 234309 (2014); 10.1063/1.4903791

A new ab initio intermolecular potential energy surface and predicted rotational spectra of the Ne−H2S complex
J. Chem. Phys. 136, 214307 (2012); 10.1063/1.4725715

Calculation of the structure, potential energy surface, vibrational dynamics, and electric dipole properties for the Xe:HI van der Waals complex
J. Chem. Phys. 134, 174302 (2011); 10.1063/1.3583817

The HOOH UV spectrum: Importance of the transition dipole moment and torsional motion from semiclassical calculations on an ab initio potential energy surface
J. Chem. Phys. 132, 084304 (2010); 10.1063/1.3317438

Interaction of lead atom with atmospheric hydroxyl radical. An ab initio and density functional theory study of the resulting complexes PbOH and HPbO
J. Chem. Phys. 121, 7207 (2004); 10.1063/1.1784431

Ab initio global potential, dipole, adiabatic, and relativistic correction surfaces for the HCN–HNC system

Tanja van Mourik
Department of Chemistry, University College London, London WC1H 0AJ, United Kingdom

Gregory J. Harris, Oleg L. Polyansky,[a)] and Jonathan Tennyson[b)]
Department of Physics and Astronomy, University College London, London WC1E 6BT, United Kingdom

Attila G. Császár
Department of Theoretical Chemistry, Eötvös University, P.O. Box 32, H-1518 Budapest 112, Hungary

Peter J. Knowles
Department of Chemistry, University of Birmingham, Edgbaston, Birmingham B15 2TT, United Kingdom

Ab initio semiglobal potential energy and dipole moment hypersurfaces for the isomerising HCN–HNC system are computed, using a grid of 242 points, principally at the all-electron cc-pCVQZ CCSD(T) level. Several potential energy hypersurfaces (PES) are presented including one which simultaneously fits 1527 points from earlier *ab initio*, smaller basis CCSD(T) calculations of Bowman *et al.* [J. Chem. Phys. **99**, 308 (1993)]. The resulting potential is then morphed with 17 aug-cc-pCVQZ CCSD(T) points calculated at HNC geometries to improve the representation of the HNC part of the surface. The PES is further adjusted to coincide with three *ab initio* points calculated, at the cc-pCV5Z CCSD(T) level, at the critical points of the system. The final PES includes relativistic and adiabatic corrections. Vibrational band origins for HCN and HNC with energy up to $12\,400$ cm^{-1} above the HCN zero-point energy are calculated variationally with the new surfaces. Band transition dipoles for the fundamentals of HCN and HNC, and a few overtone and hot band transitions for HCN have been calculated with the new dipole surface, giving generally very good agreement with experiment. The rotational levels of ground and vibrationally excited states are reproduced to high accuracy. © *2001 American Institute of Physics.*
[DOI: 10.1063/1.1383586]

I. INTRODUCTION

The [H,C,N] chemical system is of key interest for a number of reasons: It is the prototypical isomerizing system with a stable (HCN) and a metastable (HNC) isomer, both with linear geometries; the rotations and vibrations of HCN and HNC have been probed[1–4] and continue to be probed experimentally[5–7] over a wide range of excitation energies; its isomerising motion has also been subject to theoretical studies;[8–12] it is an important constituent of both the interstellar medium, where anomalously high ratios of HNC to HCN are found frequently, and of the atmosphere of cool carbon stars. Furthermore, calculations by Jørgensen and co-workers[13,14] suggest that the proper and detailed treatment of the vibration–rotation spectrum can have a profound influence on the modelling of the atmosphere of such C-stars. It is this problem which motivated the present study.

The potential energy hypersurface (PES) about the HCN minimum, and the resulting localized rovibrational energy levels, have been the subject of detailed theoretical studies.[15–18] However, at typical C-star temperatures of 2000–4000 K one would expect significant populations of both isomers necessitating a (semi)global approach. Semiglobal PESs of the [H,C,N] system have been constructed by Bowman and co-workers[19–22] and others.[23] These PESs include both pure *ab initio* surfaces and surfaces adjusted to spectroscopic data. *Ab initio* techniques employed in these studies gave, in particular, less satisfactory results for properties dependent on the C–N bond, *ab initio* calculations have also been performed on excited states of HCN–HNC, see for example, Stanton and Gauss.[24] Calculations of stellar opacities, or indeed spectra, require not only reliable PESs but also dipole moment surfaces (DMS) to give the necessary intensity information. Despite a long-running controversy over the intensity of overtone spectra of HCN[25,26] there appears to be surprisingly little work on the DMS of the [H,C,N] system. Indeed, we were able to identify only one previous DMS which covers the isomerising region, due to Jakubetz and Lan.[27] In this paper we present a semiglobal DMS of the [H,C,N] system and a number of *ab initio* PESs. These surfaces not only combine results from calculations performed at a number of different levels which allow us, for example, to determine the critical points on the surface to very high accuracy, but also include consideration of electronic relativistic effects and a simple adiabatic correction to the Born–Oppenheimer approximation, both of which are usually neglected during *ab initio* construction of PESs.[28]

Section II of this paper presents details about our *ab*

---

a)Permanent address: Institute of Applied Physics, Russian Academy of Science, Uljanov Street 46, Nizhnii Novgorod, Russia 603024.
b)Electronic mail: j.tennyson@ucl.ac.uk

initio computations and Sec. III describes our fits. Spectroscopic results obtained are presented in Sec. IV, followed by conclusions in Sec. V.

II. ELECTRONIC STRUCTURE CALCULATIONS

The majority of electronic structure calculations were performed with the MOLPRO 96[29] and the NWCHEM[30] program systems. Calculation of relativistic energies, utilizing the direct perturbation theory (DPT) approach of Kutzelnigg[31,32] in the framework of the Dirac–Coulomb Hamiltonian, were performed with a modified[33] version of the program package DALTON.[34] Determination of the diagonal Born–Oppenheimer corrections (BODC)[35] utilized the code PSI2.[36]

A. Computational details

To investigate the suitability of single-reference coupled-cluster (CC) techniques, in particular the one including single, double, and a perturbative estimate of triple excitations [CCSD(T), Ref. 37], for PES and DMS calculations for the ground electronic state of the [H,C,N] system, we have performed multireference configuration interaction (MR-CI) calculations with the cc-pVTZ basis set at three geometries chosen to be near the HCN and HNC minima and the saddle point (see Table IV below). These calculations show that (a) convergence of the energy differences with respect to the enlargement of the reference space is very slow, and (b) the MR-CI energies converge to values that are in excellent agreement with the CCSD(T) relative energy values. We can thus conclude that the CCSD(T) method is a good choice for the PES calculations. This is additionally confirmed by T_1 diagnostic values[38] from all-electron cc-pCVTZ CCSD calculations, which were found to be 0.0125, 0.0165, and 0.0220 for the HCN and HNC minima and the saddle point, respectively. These T_1 values indicate that it is adequate to use single-reference techniques to describe the portions of the ground electronic state of the [H,C,N] system of interest for us, and that the CCSD(T) method is expected to yield highly accurate energies and dipole moments with a judicious choice of basis sets.

Consequently, this study of the ground-state PES and DMS of the [H,C,N] system utilizes CCSD(T) wave functions obtained with several Gaussian basis sets. The computations of Bowman *et al.*,[20] also performed at the CCSD(T) level, employed a very extended grid comprising 2160 points. Therefore, a much smaller basis than those utilized in this study had to be employed. As it is not practical to recompute CCSD(T) energies at such an extensive grid with large basis sets, we selected grid points from Bowman *et al.* which lay less than 25 000 cm^{-1} above the absolute minimum of the surface. This selection still resulted in too many points, so only those grid points were retained for which the H–CN Jacobi angle, θ, was equal to 0, 20, 40, 60, 80, 100, 120, 140, 160, or 180°; i.e., only half of the angular grid was retained. This procedure resulted in a total of 242 points. Finally, a variety of high-accuracy *ab initio* methods were used to determine the relative energy and geometry of three stationary points of the ground-state [H,C,N] system: the two minima (HCN and HNC) and the saddle point (transition state) connecting them.

Electronic energies and dipole moments were calculated at the selected 242 grid points employing cc-pCVQZ CCSD(T) wave functions and correlating all electrons. At each grid point the dipole moment was computed via the finite-field method. To check the suitability of the grid, 14 additional energy calculations were run, at the same level, at new grid points about the HNC minimum; these points were not used in the final fit. Seventeen calculations were repeated with the larger aug-cc-pCVQZ basis also about the HNC minimum. This was done to improve the surface around the secondary minimum (see below).

B. Stationary points

Geometries of the three stationary points investigated on the ground-state PES of the [H,C,N] system were optimized at the CCSD(T) level using the (aug)-cc-p(C)VnZ correlation-consistent Gaussian basis sets of Dunning and co-workers,[39–41] where n is the cardinal number of the basis set, n is 2, 3, 4 for cc-pCVDZ, cc-pCVTZ, and cc-pCVQZ, respectively. Starting at the cc-pCV5Z/CCSD(T) level full geometry optimizations proved to be computationally prohibitive. The two bond distances of linear HCN and HNC were therefore optimized by a simple two-step line search. First the CH distance (for HCN) or the NH distance (for HNC) was optimized, keeping the CN distance fixed at an estimated value, obtained by extrapolating the cc-pCVDZ to cc-pCVQZ results using a simple three-parameter exponential function of the form

$$R(n) = A + Be^{-Cn}, \tag{1}$$

where R is the distance to be extrapolated, n is the cardinal number of the basis set, and A, B, and C are fitting parameters. Next, the CN distance was optimized, keeping the other distances fixed at their optimized values. All distances were optimized to within an accuracy of $0.0001\,a_0$. This results in an accuracy for the cc-pCV5Z CCSD(T) energy of better than $0.5\,\mu E_h$. For the saddle point, only one single-point calculation was carried out at the estimated cc-pCV5Z CCSD(T) geometry. This geometry was obtained by estimating the values of the distances by an exponential extrapolation, employing cc-pCVDZ to cc-pCVQZ results. The bond angle was kept at the cc-pCVQZ optimized value, since the angle was found to be virtually independent of the basis set employed for its determination.

Tables I–III list computed equilibrium bond lengths and total energies for HCN, HNC, and the saddle point, respectively. Also listed are the experimental equilibrium distances of the minima.[42–44]

The inclusion of diffuse functions in the cc basis sets does not significantly change the computed relative energies, as indicated by the very small difference between the cc-p(C)VnZ and aug-cc-p(C)VnZ results. Moreover, the effect decreases with increasing basis set quality: The cc-p(C)VnZ and aug-cc-p(C)VnZ results converge to the same limiting value.

For simple diatomic molecules CCSD(T) geometry optimizations with large core-valence basis sets proved to be extremely accurate (see, e.g., Ref. 45). Note, in particular, the excellent agreement between the extrapolated all-electron

TABLE I. Basis set dependence of the equilibrium distances (r_{CH} and r_{CN}) and the total energy (E_e) of HCN computed at the CCSD(T) level.[a]

Basis set	FC/AE[a]	E_e/E_h	r_{CH}/a_0	r_{CN}/a_0
cc-pVDZ	FC	−93.189 560	2.0459	2.2211
cc-pVTZ	FC	−93.275 219	2.0161	2.1923
cc-pVQZ	FC	−93.301 303	2.0161	2.1854
cc-pV5Z	FC	−93.309 331	2.0156	2.1839
Extrapolated	FC	−93.312 900		
aug-cc-pVDZ	FC	−93.204 711	2.0440	2.2220
aug-cc-pVTZ	FC	−93.281 168	2.0166	2.1923
aug-cc-pVQZ	FC	−93.303 457	2.0165	2.1860
Extrapolated	FC	−93.312 628		
cc-pCVDZ	FC	−93.193 818	2.0446	2.2184
cc-pCVTZ	FC	−93.279 132	2.0180	2.1899
cc-pCVQZ	FC	−93.302 838	2.0161	2.1850
Extrapolated	FC	−93.311 960		
cc-pCVDZ	AE	−93.268 433	2.0432	2.2171
cc-pCVTZ	AE	−93.380 461	2.0160	2.1863
cc-pCVQZ	AE	−93.414 082	2.0136	2.1805
cc-pCV5Z	AE	−93.424 144	2.0130	2.1789
Extrapolated	AE	−93.428 441	2.0128	2.1783
aug-cc-pCVDZ	AE	−93.284 449	2.0413	2.2175
aug-cc-pCVTZ	AE	−93.385 871	2.0164	2.1873
aug-cc-pCVQZ	AE	−93.416 083	2.0142	2.1811
Extrapolated	AE	−93.428 901	2.0140	2.1795
Expt. (Ref. 42)			2.0135	2.1793
Expt. (Ref. 43)			2.0141	2.1792

[a]AE=all electrons correlated, FC=frozen core calculations (only the valence electrons correlated). Extrapolations to complete basis set (CBS) limit, when reported, were performed with a three-parameter exponential form, Eq. (1), and using the best three computed values. The cc-pCV5Z optimized geometries were obtained with a simple two-step line search, see text.

TABLE II. Basis set dependence of the equilibrium distances (r_{NH} and r_{CN}) and the total energy (E_e) of HNC computed at the all-electron CCSD(T) level.[a]

Basis set	E_e/E_h	r_{NH}/a_0	r_{CN}/a_0
cc-pCVDZ	−93.243 227	1.9016	2.2474
cc-pCVTZ	−93.356 481	1.8818	2.2155
cc-pCVQZ	−93.390 047	1.8932	2.2099
cc-pCV5Z	−93.400 105	1.8807	2.2083
Extrapolated	−93.404 408		
aug-cc-pCVDZ	−93.260 925	1.9014	2.2479
aug-cc-pCVTZ	−93.362 067	1.8840	2.2171
aug-cc-pCVQZ	−93.392 185	1.8816	2.2104
Extrapolated	−93.404 957	1.8812	2.2085
Expt. (Ref. 44)		1.878	2.209

[a]See footnote a of Table I.

transition is 3.03 D, again close to the measured dipole, 3.05 D, of Blackman *et al.*[48]

Molecular properties computed with correlation-consistent basis sets generally converge monotonically toward an apparent limit;[49,50] this was found here for the computed energies and most of the time for the distances of the three stationary points investigated on the ground-state [H,C,N] PES. The only clear exception found is the NH distance in HNC computed with cc-pCVnZ basis sets, which shows an irregular convergence pattern. Such a zigzag convergence pattern is often observed for properties that are significantly affected by basis set superposition error (BSSE).[51]

It is well known that PESs of weakly bound complexes may be distorted by BSSE, and in these cases the geometry should be optimized on the counterpoise (CP)-corrected[52] surface. For covalently bound systems, like HCN, it is generally accepted that the effect of BSSE is rather small, although investigations have found evidence of BSSE in strongly bound systems.[51,53,54] To investigate if the irregular convergence of the NH distance in HNC is caused by BSSE, we have recomputed the geometries of HCN and HNC with BSSE corrections. Figure 1(a) shows that the CP-corrected NH distance does converge regularly with increasing cc-pCVnZ basis set quality, confirming that the unexpected convergence behavior of the NH distance is indeed caused by BSSE. Regular convergence is also restored by using the aug-cc-pCVnZ sets, as illustrated in Fig. 1(b). This indicates that inclusion of diffuse functions in the basis set significantly decreases the BSSE effect.

aug-cc-pCVnZ CCSD(T) and the experimental geometry parameters for HCN and HNC. Nevertheless, computation of the PES of the [H,C,N] system at the aug-cc-pCVQZ and cc-pCV5Z CCSD(T) levels is computationally too expensive. For this reason, we chose to perform our CCSD(T) calculations for the PES and DMS with the cc-pCVQZ basis set with all electrons correlated. The equilibrium distances computed at the cc-pCVQZ CCSD(T) level are in good agreement with the observed values, and the computed HCN dipole moment, 2.995 D, is close to the empirical equilibrium dipole moment, 3.016(2) D, of DeLeon and Muenter[46] and the calculated CCSD(T) dipole of 3.015 D of Botschwina *et al.*[47] Furthermore, our vibrational ground-state $J=0-1$ HNC dipole determined from the $J=0-1$

TABLE III. Basis set dependence of the equilibrium distances (r_{CH}, r_{NH}, and r_{CN}), the HCN angle (α), and the total energy (E_e) of the saddle point computed at the all-electron CCSD(T) level.[a]

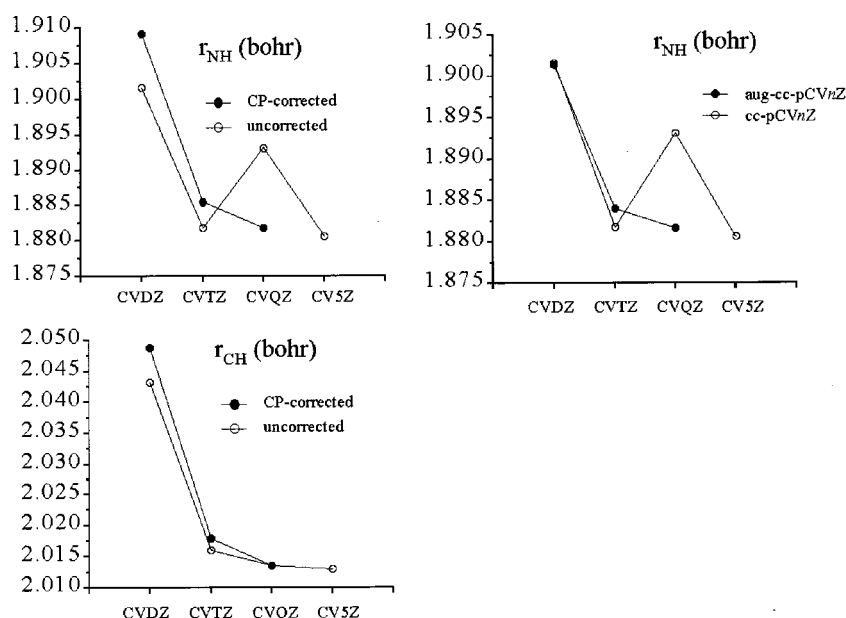| Basis set	E_e/E_h	r_{CH}/a_0	r_{NH}/a_0	r_{CN}/a_0	α/deg
cc-pCVDZ	−93.192 776	2.2571	2.6628	2.2825	71.827
cc-pCVTZ	−93.303 961	2.2376	2.6347	2.2505	71.786
cc-pCVQZ	−93.337 448	2.2365	2.6252	2.2439	71.733
cc-pCV5Z	−93.347 508	2.2365	2.6220	2.2426	71.733
Extrapolated	−93.351 828				
aug-cc-pCVDZ	−93.210 243	2.2709	2.6655	2.2845	71.623
aug-cc-pCVTZ	−93.309 817	2.2407	2.6330	2.2515	71.763

[a]See footnote a of Table I.

FIG. 1. Optimized bond lengths from CCSD(T) calculations as a function of basis set size. (a) Effect of BSSE on the convergence of the NH distance of HNC. (b) Effect of the inclusion of diffuse functions on the convergence of the NH distance of HNC. (c) Effect of BSSE on the convergence of the CH distance of HCN.

The CP-corrected as well as the uncorrected CH distances in HCN show regular convergence, as depicted in Fig. 1(c). The two curves are very close to each other and converge smoothly towards the same limit. At the cc-pCVQZ CCSD(T) level the corrected and uncorrected CH distances are identical (within the accuracy of the optimization procedure).

C. Energy separations

Table IV lists the energy separations between the three stationary points investigated. The energy differences should be better converged than the individual energies, because there will be some cancellation of errors in taking the differences. This can be seen from the effect of the diffuse functions, which is only 20–40 cm^{-1} for the energy differences.

Table V presents the results of a valence focal-point analysis[55] of the HCN–HNC and HCN–TS (saddle point) energy differences, based on coupled-cluster calculations (Series CC) performed at fixed reference geometries.

The valence-only complete basis set (CBS) CCSDT estimate for the HCN–HNC energy difference is $+5147$ cm^{-1}. We expect higher-order correlation effects, not taken explicitly into account, to be smaller than about 10–15 cm^{-1}. The core-valence correction is $+70$ cm^{-1}, computed at the aug-cc-pCVQZ CCSD(T) level. Adding relativistic and BODC corrections, $+11$ and -6 cm^{-1}, respectively (see Sec. III C below), results in a final energy difference of 5222 cm^{-1}. This energy difference, when corrected for zero-point energies (ZPE), taken to be -96 cm^{-1} (*vide infra*), becomes 5126 cm^{-1}, with a conservative error bar of about 50 cm^{-1}. This converged *ab initio* prediction is in agreement with the experimental results of Pau and Hehre,[56] who obtained 5180 ±700 cm^{-1}, rather than 3600 ± 400 cm^{-1} given by Maki *et al.*[57] The *ab initio* potential surface of Bowman *et al.*[20] gives a value of 5202 cm^{-1} for the HCN–HNC energy difference which also agrees with Pau and Hehre rather than Maki *et al.*

The valence-only CBS CCSDT energy difference between the HCN minimum and the transition state is 16 614 cm^{-1}, while the core-valence correction, obtained at the aug-cc-pCVQZ CCSD level, is $+135$ cm^{-1}. Adding relativistic and BODC corrections of -24 and $+8$ cm^{-1} (see Sec. III C), we arrive at the converged *ab initio* estimate of 16 733 cm^{-1} for the isomerization barrier. This number may be compared to the previous, inferior theoretical estimates of the isomerization barrier: 15 600 cm^{-1} of Lee and Rendell,[58] 12 171 cm^{-1} of Murrell *et al.*,[23] and 16 866 cm^{-1} for the *ab initio* surface of Bowman *et al.*[20]

D. Auxiliary corrections

It has been found that electronic relativistic effects and the adiabatic or Born–Oppenheimer diagonal correction (BODC) can have a small but significant effect on the effective potential surface, and hence on the calculated vibration–rotation levels of small molecules.[50,59,60] Therefore, they have been considered as part of this study. Electronic relativistic corrections were obtained using all-electron aug-cc-pCVDZ CCSD(T) wave functions and the DPT approach of Kutzelnigg.[31,32] BODC energy points were computed at the TZ2P restricted Hartree–Fock (RHF) level. All these calculations were performed for 242 geometries representing our initial grid. The results of the *ab initio* calculations at these points for the potential energy, relativistic correction, and BODC can be obtained from the electronic archive.[61]

III. FITTED POTENTIAL ENERGY AND DIPOLE SURFACES

The function we chose to represent the [H,C,N] ground-state PES is

$$V(R,r,\gamma) = \sum_{i,j,k} A_{ijk} X^i(R,r,\gamma) Y^j(r,\gamma) P_k(\cos\gamma), \quad (2)$$

TABLE IV. The bond distances (R and r in a_0) and the relative energy (V/cm^{-1}) of the minima and saddle points of various *ab initio* potential energy surfaces and sets of potential points. Energy of the HCN minimum is set to zero in all cases.

Surface	HCN		HNC			Barrier			
	R	r	R	r	V	γ	R	r	V
CCSD(T) calculations (optimized geometries)									
cc-pCVDZ	3.2371	2.2171	2.9387	2.2474	5532	1.3306	2.2079	2.2825	16 605
cc-pCVTZ	3.1934	2.1863	2.9042	2.2155	5263	1.3342	2.1864	2.2505	16 790
cc-pCVQZ	3.1879	2.1805	2.9130	2.2099	5275	1.3363	2.1836	2.2439	16 819
cc-pCV5Z	3.1864	2.1789	2.8997	2.2083	5276	1.3366	2.1834	2.2426	16 820
aug-cc-pCVDZ	3.2355	2.2175	2.9388	2.2479	5163	1.3365	2.2156	2.2845	16 286
aug-cc-pCVTZ	3.1943	2.1873	2.9072	2.2171	5224	1.3350	2.1887	2.2515	16 692
aug-cc-pCVQZ	3.1887	2.1811	2.9017	2.2104	5245				
cc-pCVQZ Points[c]	3.1667	2.1333	2.8333	2.2444	5533	1.3963	2.1667	2.2444	16 445
cc-pCV5Z Points[d]	3.1864	2.1789	2.8998	2.2083	5276	1.3347	2.1826	2.2425	16 820
cc-pVTZ MRCI[a] and CCSD(T) calculations (fixed geometries)									
MRCI(9,2/2)	3.1704	2.1430	2.8752	2.1845	4847	1.5708	2.4368	2.2053	14 171
MRCI(10,2/2)					5202				14 316
MRCI(11,3/2)					5210				14 341
MRCI+Q(11,3/2)					5089				14 244
CCSD(T)					5065				14 300
Potential surfaces									
Bowman *et al.*[b]	3.198	2.196	2.902	2.220	5202	1.3224	2.1873	2.2558	16 843
VCVQZ	3.1888	2.1806	2.9003	2.2097	5262	1.3650	2.1595	2.2464	16 754
VQZANO1	3.1879	2.1805	2.9020	2.2101	5284	1.3522	2.1687	2.2463	16 784
VQZANO2	3.1857	2.1789	2.9005	2.2085	5275	1.3347	2.1826	2.2425	16 819
VQZANO+	3.1855	2.1785	2.9003	2.2081	5281	1.3338	2.1828	2.2421	16 798
Expt.[e]	3.1869	2.1792	2.8979	2.2089	⋯	⋯	⋯	⋯	⋯
Expt.[f]	3.1871	2.1792	⋯	⋯	⋯	⋯	⋯	⋯	⋯

[a]MRCI($n,m/2$) indicates an active space that includes the 3-n A′ and 1-m A″ orbitals (the lowest 2 A′ orbitals are not correlated).
[b]Potential surface of Bowman *et al.* (Ref. 20).
[c]Points are not optimized to minima and saddle point but are the points closest to the minima and saddle point on our grid of points.
[d]Optimized to lie at the critical points.
[e]Experimentally determined equilibrium bond lengths determined using isotopic substitution (Refs. 42 and 44).
[f]Equilibrium bond lengths determined from spectroscopic fit (Ref. 18).

where (R,r,γ) are Jacobi coordinates ($R=r_{H-CN}$, $r=r_{CN}$), with HCN at $\gamma=0$. A_{ijk} is a constant for a particular i, j, and k, and $P_k(\cos\gamma)$ are Legendre polynomials for the angular (γ) component of the fit. X and Y are functions of primarily the R and r coordinates, respectively, and are based on Morse coordinate transformations,[17] with

$$X(R,r,\gamma)=1-e^{-\alpha_R(\gamma)[R-R_e(\gamma,r)]}, \qquad (3)$$

$$Y(r,\gamma)=1-e^{-\alpha_r[r-r_e(\gamma)]}. \qquad (4)$$

The position of the minimum in r and R and the steepness of the potential in R are not constant with the change of γ, hence we have made R_e, r_e, and α_R a function of γ. R_e also shows a less strong but significant dependence on r, hence we also made R_e a function of r^2. The functions R_e, r_e, and α are

$$R_e(\gamma,r)=A_{R_e}+B_{R_e}\cos\gamma+C_{R_e}\cos^2\gamma+D_{R_e}r^2\cos^2\gamma, \qquad (5)$$

$$r_e(\gamma)=A_{r_e}+B_{r_e}\cos\gamma+C_{r_e}\cos^2\gamma, \qquad (6)$$

$$\alpha_R(\gamma)=A_{R_\alpha}+B_{R_\alpha}\cos\gamma+C_{R_\alpha}\cos^2\gamma, \qquad (7)$$

with α_r a constant.

Initially the functions $R_e(\gamma,r)$ and $r_e(\gamma)$ were fitted to the least energy isomerization (LEI) path. However, if we

allowed the parameters of these functions to change we were able to achieve a lower standard deviation for the fit to the overall potential energy surface. This functional form yielded a fit to the initial 242 *ab initio* potential points calculated in this work with a standard deviation of less than 3 cm^{-1}. There are 180 terms in this fit with $i_{max}=4$, $j_{max}=5$, and $k_{max}=5$. This fit shall be hereafter referred to as the VCVQZ potential surface. Using 216 terms and maximum values of i, j, and k of 5 in our fitting function, we also achieved a standard deviation of 3 cm^{-1} to the (unshifted) points of Bowman *et al.*[20] truncated at 25 000 cm^{-1}, a total of 508 points. This fit will be hereafter referred to as the VANO25 fit.

The HCN and HNC minima and the LEI path of the VCVQZ surface occur at significantly different geometries and energies than those characterising the surface of Bowman *et al.*,[20] resulting in large standard deviations (>800 cm^{-1}) when both grids were simultaneously fitted. This problem was solved by "shifting" the potential points of Bowman *et al.* in the r and R coordinates and in energy as a function of the angle γ, so that the LEI path of both sets of points were coincident. This was achieved as follows: We calculated the energy, the r, and the R coordinates of the LEI path of the VANO25 surface, and those of the VCVQZ surface, at 40 equally spaced values over the range $0 \leqslant \gamma \leqslant \pi$. We

TABLE V. Valence focal-point analysis of the energy difference between the HCN and HNC minima and the energy difference between the HCN minimum and the saddle point (TS).[a]

Series CC HCN–HNC	ΔE_e(RHF)	δ[MP2]	δ[CCSD]	δ[CCSD(T)]	δ[CCSDT]	ΔE_e(CC)
cc-pVDZ (33)	3778	+2774	−1138	+103	−63	+5454
aug-cc-pVDZ (55)	3500	+2629	−1117	+68	−55	+5026
cc-pVTZ (74)	3464	+2762	−1142	+136	−69	+5152
cc-pCVTZ (100)	3479	+2753	−1140	+138	[−69]	
aug-cc-pVTZ (115)	3424	+2766	−1117	+119	−68	+5123
cc-pVQZ (140)	3415	+2771	−1135	+135	[−68]	
cc-pCVQZ (198)	3414	+2783	−1137	+138	[−68]	
aug-cc-pVQZ (206)	3391	+2782	−1132	+130	[−68]	
cc-pV5Z (237)	3398	+2797	−1134	+136	[−68]	
aug-cc-pCVQZ (264)	3390	+2785	−1132	+133	[−68]	
aug-cc-pV5Z (334)	3391	+2801	−1134	+134	[−68]	
CBS	3392	+2823	−1136	+138	−68	+5147
HCN–TS						
cc-pVDZ (33)	16 329	+1765	−1440	−143	−44	+16 467
aug-cc-pVDZ (55)	16 084	+1689	−1422	−162	−42	+16 146
cc-pVTZ (74)	16 465	+1729	−1382	−120	−54	+16 637
cc-pCVTZ (100)	16 480	+1701	−1380	−120	[−54]	
aug-cc-pVTZ (115)	16 410	+1694	−1374	−129	−54	+16 548
cc-pVQZ (140)	16 435	+1772	−1393	−126	[−54]	
cc-pCVQZ (198)	16 431	+1759	−1389	−124	[−54]	
aug-cc-pVQZ (206)	16 406	+1763	−1388	−129	[−54]	
cc-pV5Z (237)	16 420	+1779	−1399	−129	[−54]	
aug-cc-pCVQZ (264)	16 404				[−54]	
aug-cc-pV5Z (334)	16 409	+1783	−1401	[−129]	[−54]	
CBS	16 412	+1795	−1410	[−129]	−54	+16 614

[a]The number of contracted Gaussian functions in each basis set is indicated in parentheses. The reference geometries for all focal-point calculations were chosen as follows:
(i) $r_{CH}=2.0137\,a_0$ and $r_{CN}=2.1806\,a_0$ for HCN;
(ii) $r_{NH}=1.8820\,a_0$ and $r_{CN}=2.2100\,a_0$ for HNC; and
(iii) $r_{CH}=2.2425\,a_0$ $r_{CN}=2.2463\,a_0$, and HCN=1.235 rad for the saddle point (TS).Basis set extrapolations were performed (Ref. 50) with Eq. (1) for the RHF energies and $E_X=E_{CBS}+b*X^{-3}$ for the correlation energy, where X is the cardinal number of the correlation-consistent (cc) basis and only the best three–two energies were used during the extrapolation. The higher-order correlation increments listed in brackets are taken for the purpose of extrapolation from corresponding entries for smaller basis sets.

then used a Legendre polynomial up to fifth-order to least-squares fit the differences between coordinates and energy of the VANO25 and the VCVQZ surfaces. With these functions the points of Bowman *et al.* were shifted at all values of the angle γ. We fitted the shifted Bowman *et al.* points truncated at 25 000 cm^{-1}, hereafter referred to as the VANO25S surface. The steepness of the slope of the potential with change of the r coordinates of the VANO25S surface was less than that of the VCVQZ surface, resulting in a large difference in energy (200 cm^{-1}) between the two surfaces at high deviations of r from the local minimum. A weighting system was chosen for all the points, to reflect the accuracy of, and the differences between, the shifted points of Bowman *et al.* and the points of this work, and the greater importance of fitting accuracy at low energies. We gave a weight of 5000 to all the points calculated in this work. The weight, W, of the shifted Bowman *et al.* points was calculated from a function based on the inverse square of the displacement of r from the $r_e(\gamma)$ on the LEI path

$$W(r,V)=\frac{w(V)}{1+(200(r-r_e(\gamma))^2)},\qquad (8)$$

where W is the weight given to the point and $w(V)$ is a further weighting factor as a condition of energy, given by

$$V<25\,000\ \text{cm}^{-1},\quad w(V)=100,$$

$$25\,000\ \text{cm}^{-1}\leqslant V<35\,000\ \text{cm}^{-1},\quad w(V)=10,$$

$$V\geqslant 35\,000\ \text{cm}^{-1},\quad w(V)=0.5.$$

The shifted Bowman *et al.* points were truncated at 45 700 cm^{-1}, the dissociation energy of HCN,[62] so that the very high-energy points did not interfere with the fit at low energies. This weighting method was used to least-squares fit the potential points calculated in this work and the remaining 1527 shifted points of Bowman *et al.* We used 252 terms with i_{max} and j_{max} of 5 and a k_{max} of 6. The fit, hereafter referred to as the VQZANO1 surface, had an RMS deviation of 3.3 cm^{-1} from the points calculated in this work, an over-all standard deviation of 412 cm^{-1}, and an root-mean-square (rms) deviation of 376 cm^{-1}.

A. Morphing the potential energy hypersurface

The vibrational fundamentals of both HCN and HNC, calculated with the VQZANO1 potential surface deviate by 4 cm^{-1} or less from the observed band origins except for the HN stretching fundamental (ν_1) of HNC (see Tables VI and VII). This calculated fundamental value deviates from the observed value by 20 cm^{-1}, an anomalously large deviation.

Extra points calculated at the CCSD(T)/cc-pCVQZ level in the region of the HNC minimum made little difference to band origins suggesting that this was not a problem with the coarseness of our grid. However, we found that the cc-pCVQZ basis used to calculate our points is too small to model the HNC part of the potential accurately. With our limited computer time 17 new *ab initio* points at the level aug-cc-pCVQZ CCSD(T) were calculated, see Sec. II. We then adapted our initial potential by "morphing" it[63,64] using the function

$$V_{\text{morph}}(R, r, \gamma) = V_{\text{orig}}(R + \rho(R, \gamma), r, \gamma). \tag{9}$$

Here V_{morph} is the morphed surface, V_{orig} is the original surface, and $\rho(R, \gamma)$ is a distance scaling function

$$\rho(R, \gamma) = \alpha(\gamma) \sum_i \sum_j B_{ij} (R - R_{\text{LEI}}(\gamma))^i \cos^j(\gamma), \tag{10}$$

where B_{ij} are the coefficients of the fit and $R_{\text{LEI}}(\gamma)$ is the local R coordinate of the LEI path and $\alpha(\gamma)$ is a damping function with the conditions $\alpha(\gamma) \rightarrow 0$ when $\gamma \rightarrow 0$ and $\alpha(\gamma) \rightarrow 1$ when $\gamma \rightarrow \pi$. The damping function was used to force $\rho(R, \gamma)$ to zero at the low angles that correspond to the HCN side of the surface. The functional form for $\alpha(\gamma)$ is given by

$$\alpha(\gamma) = \exp(-(0.6(\gamma - \pi))^6). \tag{11}$$

We used Eq. (9) with nine terms and $i_{\text{max}} = 2$ and $j_{\text{max}} = 2$ to morph the VQZANO1 surface with the 17 new, more accurate points. The morphed surface has a standard deviation of 4 cm^{-1} for the 17 new aug-cc-pCVQZ points. The HNC HN stretching fundamental calculated from the morphed surface improved to within 14 cm^{-1} of the experimental value. The other vibrational fundamentals calculated from the morphed surface are almost unchanged from those calculated with the VQZANO1 surface, as we intended.

B. Stationary points

Finally the potential was re-mapped so that the minima and saddle point were coincident in energy and coordinates with the three cc-pCV5Z points calculated at the critical points. Coordinate mappings for R, r, and γ and an energy scaling function were least-squares fitted to the three high-accuracy points with the coordinates and energy of the minima and saddle point of the morphed surface. The functional forms for these mappings and energy scaling function are as follows:

$$r_{\text{map}} = r_{\text{orig}} + A_r + B_r f^4(\gamma), \tag{12}$$

$$R_{\text{map}} = R_{\text{orig}} + A_R + B_R f^4(\gamma), \tag{13}$$

$$\gamma_{\text{map}} = \gamma_{\text{orig}} + B_\gamma f^{16}(\gamma), \tag{14}$$

$$V_{\text{scale}} = V_{\text{orig}} + A_V g(\gamma) + B_V f^{16}(\gamma). \tag{15}$$

In these equations A and B are the coefficients of the mapping fit and $f(\gamma)$ and $g(\gamma)$ are functions of the angle γ. The R and r coordinates of the three high-accuracy points and the R and r coordinates of the minima and saddle point in our potential deviate by the greatest amount at the saddle point ($\gamma = 1.3347$). The deviations in R and r at the HCN minimum are roughly the same as those at the HNC minimum. A function for $f(\gamma)$ that would peak at $\gamma = 1.3347$ while $f(\gamma) = 0$ when $\gamma = 0$ and $\gamma = \pi$ was chosen. The function used in this work is

$$f(\gamma) = \sin \gamma + 0.131\,325 \sin(2\gamma). \tag{16}$$

We chose the 4th power of $f(\gamma)$ in Eqs. (12) and (13) to "sharpen" the peak so that the mapping at the saddle point would not influence the HCN and HNC minima regions. The γ mapping function (14) should be 0 at $\gamma = 0$ and $\gamma = \pi$. For the energy scaling the damping function (16) was used, with a $g(\gamma)$ function where $g(\gamma) = 0$ for HCN geometries and $g(\gamma) \neq 0$ for HNC geometries. The $g(\gamma)$ function used in this work is

$$g(\gamma) = \tan^{-1}[15(\gamma - 1.2)] + \pi/2. \tag{17}$$

The above functions were used to map and energy scale the VQZANO1 surface to the three high-accuracy points at the minima and saddle point. The mapped VQZANO1 surface will be referred to as the VQZANO2 surface hereafter.

C. The relativistic and BODC correction fits

Both the relativistic energy correction and BODC points were least-squares fitted with the function

$$C(R, r, \gamma) = \sum_i \sum_j \sum_k A_{ijk} R^i r^j P_k^0(\cos \gamma). \tag{18}$$

This surface proved to be far smoother than the potential energy surface, so only 80 coefficients with $i_{\text{max}} = 3$, $j_{\text{max}} = 3$, and $k_{\text{max}} = 4$ were required to fit to the relativistic correction points with a standard deviation of 0.3 cm^{-1}. The relativistic correction is $+5.86$ cm^{-1} at the HCN minimum, $+17.26$ cm^{-1} at the HNC minimum, and -16.77 cm^{-1} at the saddle point. For the BODC surface we used $i_{\text{max}} = 2$, $j_{\text{max}} = 3$, and $k_{\text{max}} = 4$, which yielded a standard deviation of 0.93 cm^{-1}. The BODC is -1.65 cm^{-1} at the HCN minimum, -7.64 cm^{-1} at the HNC minimum, and $+6.37$ cm^{-1} at the saddle point. Figure 2 shows a contour plot of our VQZANO2 potential surface with relativistic and BODC corrections (referred to as VQZANO+surface) in R and γ, with r fixed to the equilibrium value of $2.1785\,a_0$.

D. Fitting the dipole moment surface

The x and z components of the 242 *ab initio* dipole points of this work were least-squares fitted using functions similar to those used by Brocks *et al.*[65] to represent the dipoles of KCN and LiCN,

$$\mu_z(R, r, \gamma) = \sum_i \sum_j \sum_{k=0}^{k_{\text{max}}} A_{ijk} \exp(B_i R) \exp(C_j r) P_k^0(\cos \gamma), \tag{19}$$

TABLE VI. Calculated HCN $l=0$ and $J=0$ pure vibrational band origins, relative to HCN zero-point energy.

ν_1	ν_2	ν_3	VQZANO+	VQZANO2	VQZANO1	Bowman et al. (Ref. 20)	Expt.[a]
0	0	0	3481.46[b]	3482.16[b]	3481.69[b]	3477.4[b]	
0	2	0	1414.92	1415.06	1414.24	1418.9	1411.42
0	0	1	2100.58	2100.93	2100.93	2090.3	2096.85
0	4	0	2801.46	2801.80	2800.14	2812.5	2802.96
1	0	0	3307.75	3308.61	3308.71	3334.1	3311.48
0	2	1	3510.99	3511.39	3510.58	3507.4	3502.12
0	6	0	4176.24	4176.80	4174.05	4178.0	4174.61
0	0	2	4181.45	4182.14	4182.14	4161.5	4173.07
1	2	0	4686.29	4687.24	4687.08	4703.4	4684.31
0	4	1	4891.76	4892.26	4890.61	4899.9	4888.00
1	0	1	5394.43	5395.67	5395.77	5399.4	5393.70
0	8	0	5537.76	5538.56	5534.28	5532.3	5525.81
0	2	2	5586.50	5587.13	5586.32	5570.5	5571.89
1	4	0	6033.72	6034.83	6034.75	6054.0	6036.96
0	0	3	6242.42	6243.43	6243.43	6211.4	6228.60
0	6	1	6260.59	6261.22	6258.49	6256.5	6254.38
2	0	0	6513.50	6515.23	6515.43	6553.2	6519.61
1	2	1	6768.51	6769.74	6769.57	6765.5	6761.33
0	10	0	6879.60	6880.72	6874.10	6873.5	6855.53
0	4	2	6960.99	6961.60	6959.97	6958.5	6951.68
1	6	0	7369.18	7370.47	7370.39	7390.3	···
1	0	2	7461.60	7463.19	7463.28	7445.7	7455.42
0	8	1	7617.24	7618.06	7613.76	7600.6	···
0	2	3	7641.28	7642.09	7641.28	7609.4	···
2	2	0	7855.84	7857.60	7858.08	7878.8	7853.51
1	4	1	8110.25	8111.54	8111.44	8115.2	8107.97
0	12	0	8197.55	8199.04	8188.72	8185.3	···
0	0	4	8283.37	8284.68	8284.68	8239.7	···
0	6	2	8323.52	8324.18	8321.47	8308.3	···
2	0	1	8584.74	8586.88	8587.08	8595.9	8585.58
1	8	0	8691.67	8693.18	8692.59	8710.3	···
1	2	2	8830.27	8831.73	8831.55	8806.2	8816.00
0	10	1	8954.47	8955.52	8948.84	8935.0	···
0	4	3	9009.00	9009.68	9008.06	8990.5	8995.22
2	4	0	9164.08	9165.95	9167.39	9188.5	···
1	6	1	9440.12	9441.50	9441.36	9441.3	···
0	14	0	9488.54	9490.47	9474.37	9470.3	···
1	0	3	9508.91	9510.83	9510.92	9474.5	9496.44
3	0	0	9619.29	9621.88	9622.16	9668.3	9627.09
0	2	4	9674.67	9675.46	9671.22	9624.3	···
0	8	2	9675.25	9676.17	9675.33	9644.9	···
2	2	1	9922.92	9924.98	9925.45	9918.1	9914.4
1	10	0	9993.95	9995.76	9993.57	10 010.0	···
1	4	2	10 165.6	10 167.0	10 166.9	10 152.3	···
0	12	1	10 266.4	10 267.8	10 257.3	10 237.7	···
0	0	5	10 304.1	10 305.7	10 305.7	10 246.8	···
0	6	3	10 364.9	10 365.6	10 362.9	10 334.0	···
2	6	0	10 460.5	10 462.6	10 465.0	10 488.9	···
2	0	2	10 636.7	10 639.2	10 639.4	10 623.7	10 631.4
0	16	0	10 749.7	10 752.1	10 727.4	10 724.2	···
1	8	1	10 758.0	10 759.6	10 758.8	10 755.3	···
1	2	3	10 871.1	10 872.7	10 872.5	10 826.4	···
3	2	0	10 925.3	10 927.8	10 928.9	10 951.0	···
0	10	2	11 006.5	11 007.5	11 000.8	10 971.4	10 974.2
0	4	4	11 035.7	11 036.4	11 034.8	10 997.7	11 015.9
2	4	1	11 225.9	11 227.9	11 229.4	11 229.2	···
1	12	0	11 271.7	11 273.9	11 268.2	11 279.5	···
1	6	2	11 489.4	11 490.8	11 490.6	11 467.5	···
0	14	1	11 536.1	11 538.1	11 535.0	11 514.6	···
1	0	4	11 549.6	11 551.4	11 550.3	11 487.4	11 516.6
3	0	1	11 672.8	11 675.9	11 676.2	11 686.9	11 674.5
0	2	5	11 688.1	11 689.1	11 688.3	11 617.6	···
0	8	3	11 710.1	11 710.8	11 706.6	11 664.3	···
2	8	0	11 744.5	11 746.6	11 751.8	11 770.2	···
2	2	2	11 969.9	11 967.9	11 972.6	11 939.9	···
0	18	0	11 977.7	11 980.8	11 944.0	11 939.8	···
1	10	1	12 055.7	12 057.5	12 055.1	12 051.4	···
1	4	3	12 192.5	12 194.9	12 197.0	12 166.6	···
3	4	0	12 200.6	12 202.2	12 202.7	12 221.5	···
0	0	6	12 304.5	12 306.3	12 302.4	12 233.8	···
0	12	2	12 311.7	12 313.0	12 306.3	12 265.7	···
0	6	4	12 382.0	12 385.3	12 387.7	12 334.8	···

[a]References 1, 2, 4–6.
[b]The HCN zero-point energy for given surface.

TABLE VII. Calculated HNC $l=0$ and $J=0$ pure vibrational band origins, relative to HNC zero-point energy.

ν_1	ν_2	ν_3	VQZANO+	VQZANO2	VQZANO1	Bowman *et al.* (Ref. 20)	Expt.[a]
0	0	0	5185.64[b]	5180.27[b]	5183.40[b]	5023.2[b]	...
0	2	0	941.917	942.541	942.601	919.9	...
0	4	0	1903.10	1904.61	1904.67	1895.5	...
0	0	1	2024.95	2025.29	2025.54	2024.6	2023.88
0	6	0	2834.81	2837.40	2837.32	2858.8	...
0	2	1	2955.05	2955.92	2956.24	2929.2	...
1	0	0	3665.10	3666.55	3672.35	3599.1	3652.68
0	8	0	3759.86	3763.67	3763.16	3794.7	...
0	4	1	3902.41	3904.11	3904.45	3892.2	...
0	0	2	4029.21	4029.89	4030.44	4024.4	...
1	2	0	4558.15	4560.11	4567.20	4507.1	...
0	10	0	4679.69	4684.95	4683.85	4727.3	...
0	6	1	4820.95	4823.73	4823.90	4832.8	...
0	2	2	4946.74	4947.86	4948.47	4912.6	...
1	4	0	5469.23	5471.98	5480.24	5440.7	...
0	12	0	5568.34	5575.51	5573.89	5638.0	...
1	0	1	5676.51	5678.3	5684.39	5628.7	5664.85
0	8	1	5736.39	5740.4	5740.12	5752.6	...
0	4	2	5879.59	5881.49	5882.1	5862.4	...
0	0	3	6012.87	6013.89	6014.76	5999.1	...
1	6	0	6354.07	6358.05	6354.99	6337.0	...
0	14	0	6404.38	6413.83	6411.88	6482.6	...
1	2	1	6558.72	6561.02	6566.03	6518.2	...
0	10	1	6646.85	6652.35	6651.51	6676.6	...
0	6	2	6784.63	6791.92	6788.03	6781.6	...
0	2	3	6917.05	6918.4	6919.33	6871.3	...
2	0	0	7189.47	7192.43	7199.25	7116.7	7171.41
0	16	0	7199.11	7208.06	7205.92	7279.9	...
1	8	0	7226.47	7231.44	7240.87	7225.5	...

[a]References 70 and 71.
[b]The energy of the HNC (0,0,0) state relative to the HCN zero-point energy.

$$\mu_x(R,r,\gamma)=\sum_i \sum_j \sum_{k=1}^{k_{max}} A_{ijk}\exp(B_iR)\exp(C_jr)P_k^1(\cos\gamma). \tag{20}$$

The z axis of our dipole surface lies along the CN bond and the x axis lies perpendicular to the x axis so that the H nucle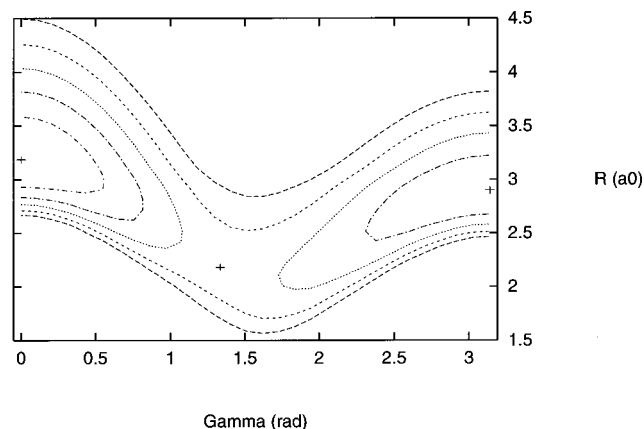us bends in the xz plane. For μ_z, we used $i_{max}=2$, $j_{max}=2$, and $k_{max}=6$ and achieved a standard deviation of 0.008 D during the fit. For μ_x, we used $i_{max}=2$, $j_{max}=2$, and $k_{max}=5$ and achieved a standard deviation of 0.002 D. The dipole points of this work are limited to nuclear geometries that correspond to energies of less than 25 000 cm^{-1}; consequently, the dipole moment surfaces (DMSs) can only be considered reliable for energies below this value.

Values for the various constants necessary to generate the VQZANO+ PES and DMS, and FORTRAN subroutines representing the surfaces, are given in the electronic archive.[61]

IV. NUCLEAR MOTION CALCULATIONS

Our vibrational, rotational, and dipole transition calculations were performed with the DVR3D program suite,[66] which uses an exact kinetic-energy (EKE) operator and a discrete variable representation (DVR) for the vibrational motions. Jacobi coordinates were used with Legendre polynomials to give the angular grid points and Morse oscillatorlike functions for the radial grids. 40 grid points were used for the R coordinate, 25 for the r coordinate and 50 for the angular coordinate. This was sufficient to converge all calculations reported here.

A. HCN and HNC band origins

We have calculated all ($J=0$) vibrational band origins (VBOs) for HCN and HNC states below 12 400 cm^{-1} rela-

FIG. 2. Contour plot of HCN–HNC VQZANO+ surface in R and γ coordinates with r fixed to the near HCN equilibrium value of 2.179 a_0. The contours have a minimum value of 5000 cm^{-1} and a maximum value of 25 000 cm^{-1}, with increments of 5000 cm^{-1}. The HCN and HNC minima and barrier are at $\gamma=0$, $\gamma=\pi$ rad, and $\gamma=1.3338$ rad, respectively, and their coordinates are marked by crosses.

TABLE VIII. Calculated HCN rotational–vibrational energy levels, relative to the zero-point energy of HCN.

$(\nu_1\nu_2^l\nu_3)$	J	VQZANO+	VQZANO1	Expt.[a]	Obs.−calc.[b]
(00^00)	1	2.959	2.954	2.956	−0.0005
	5	44.39	44.31	44.32	−0.08
	10	162.72	162.44	162.54	−0.18
	15	354.94	354.32	354.58	−0.36
	20	620.93	619.87	620.34	−0.59
$(01^1{}^e0)$	1	718.85		714.94	$(-3.91)^c$
	5	760.27		756.29	−0.06
	10	878.60		874.51	−0.18
	15	1070.80		1066.51	−0.38
	20	1336.77		1332.22	−0.64
(00^01)	1	2103.52		2099.78	−0.01
	5	2144.67		2140.87	−0.07
	10	2262.21		2258.28	−0.20
	15	2453.14		2449.01	−0.40
	20	2717.33		2712.93	−0.67
(10^00)	1	3310.68		3314.41	0.00
	5	3351.83		3355.49	−0.07
	10	3469.34		3472.88	−0.19
	15	3660.23		3663.56	−0.40
	20	3924.38		3927.42	−0.69

[a]Experimental data (Refs. 5, 72, and 73).
[b]Obs.−calc. for VQZANO+ results corrected for the vibrational error.
[c]The lowest rotational state for $(01^1{}^e0)$, taken as vibrational error.

tive to the HCN zero-point energy. Results calculated with our *ab initio* VQZANO+, VQZANO2, and VQZANO1 surfaces are reported in Tables VI and VII. These results agree well with experiment, the HCN and HNC fundamentals agree to within 4 cm^{-1} except the ν_1(HNC) fundamental. The morphed VQZANO2 surface shows an improvement over the unmorphed VQZANO1 surface, cutting the value of $E_{\mathrm{obs}}-E_{\mathrm{calc}}$ by 1/3. This shows that the 17 aug-cc-pCVQZ CCSD(T) points used made a significant difference to the cc-pCVQZ CCSD(T) surface, implying that the electronic structure of HNC needs a basis larger than cc-pCVQZ to calculate its electronic structure accurately.

Our HCN and HNC *ab initio* VBOs are significantly closer to experiment than the *ab initio* VBOs of Bowman *et al.*, especially for the HNC band origins and the HCN levels containing excited CH stretch. The better agreement of our HNC band origins again shows the need for using a larger Gaussian basis for HNC geometries. For bending states with $\nu_2 < 8$, the results from our surfaces are closer to experiment than the band origins calculated by Bowman *et al.* However, for bending states with $\nu_2 \geq 8$ the VQZANO1 surface gives results that are of comparable accuracy to those of Bowman *et al.*, but the VQZANO+ and VQZANO2 surfaces give VBOs that are roughly 5 cm^{-1} further from the experimental values. This increase in error in our results is caused by the change in coordinates of the HCN minimum in the three point mapping. There is some cancellation of error in the bend and CN stretch combination band origins of Bowman *et al.* with $\nu_1 = 0$, $\nu_2 \geq 8$, $\nu_3 \geq 1$.

B. HCN and HNC rotational energy levels

The HCN and HNC $J = 1$, 5, 10, 15, 20 pure rotational states have been calculated with the VQZANO1 and VQZANO+ surfaces, see Tables VIII and IX. The rotational

term values obtained for both surfaces show good agreement with the experimental values, showing that our surface is accurate for the calculation of rotational states. The three-point mapping has improved the rotational levels for both HCN and HNC. Particularly notable is the improvement in the CN bond length in our calculations compared to those of Bowman *et al.*, which is reflected in an improved representation of the rotational motion.

We have also calculated rovibrational energy levels for the fundamental bands of HCN and HNC using the VQZANO+ surface, see Tables VIII and IX. The obs.−calc. for these levels have been calculated and corrected for the known vibrational error, the rotational errors are, as for the pure rotational levels, less than 0.7 cm^{-1} for the $J=20$ state. This small error makes the surface useful for spectroscopic line assignments.

C. HCN and HNC band transition dipoles

Wave functions for $0 \leq J < 4$ states calculated with the VQZANO+ potential surface and the DVR3D program suite were used to compute transition dipoles using our dipole surface. Band dipole strengths can be calculated from the line dipole strengths by dividing the line dipole by the square root of the appropriate Hönl–London factors[67,68] for a particular transition dipole. There is a difference in the Hönl–London factors used in various works: Smith *et al.*[1] use Hönl–London factors that are a factor of 4 and 2 greater than those of Maki *et al.*[68] for the Π–Σ and Σ–Π bands, respectively. This in turn will give band dipoles that are a factor of $1/2$ and $1/\sqrt{2}$ the band dipoles calculated with the Hönl–London factors used by Maki *et al.*, for the Π–Σ and Σ–Π bands, respectively. To compare *ab initio* and experimental dipole band strengths it is necessary to know which Hönl–London factor was used to calculate the experimental dipole

TABLE IX. Calculated HNC rotational–vibrational energy levels, relative to HNC (0,0,0) $J=0$ state.

$(\nu_1 \nu_2^l \nu_3)$	J	VQZANO+	VQZANO1	Expt.[a]	Obs.−calc.[b]
(00^00)	1	3.021	3.025	3.042	0.02
	5	45.36	45.29	45.36	0.00
	10	166.29	166.02	166.29	0.00
	15	362.72	362.11	362.72	0.00
	20	634.52	633.45	634.50	0.02
$(01^1{}^e0)$	1	468.15		465.74	$(-2.41)^c$
	5	510.48		508.07	0.00
	10	631.38		628.97	0.00
	15	827.77		825.36	0.00
	20	1099.50		1097.09	0.00
(00^01)	1	2027.95		2026.86	−0.02
	5	2069.98		2068.88	−0.03
	10	2190.05		2188.92	−0.06
	15	2384.92		2383.89	0.04
	20	2654.92		2653.66	−0.19
(10^00)	1	3667.97		3655.66	0.11
	5	3710.13		3697.72	0.01
	10	3830.34		3817.85	−0.07
	15	4025.56		4012.98	−0.16
	20	4295.63		4282.97	−0.24

[a]Experimental data (Refs. 71 and 74).
[b]Obs.−calc. for VQZANO+ results corrected for the vibrational error.
[c]The lowest rotational state for $(01^1{}^e0)$, taken as vibrational error.

band strength and use the same factor to calculate the *ab initio* band dipole. In this work we employ the Hönl–London factors used by Maki *et al.* which we have rederived from the matrix elements given by Gordy and Cook.[69]

Jørgensen *et al.*[13] computed, at the CASSCF level with a $(C-N,H)=(5s4p2d,3s1p)$ basis set the frequencies and integrated band intensities of eight HCN bands. We have calculated the band transition dipole for these eight HCN bands, the $(02^20)-(01^10)$ HCN band and the HNC fundamental bands, using rotational transitions with $0 \leqslant J < 4$, see Tables X and XI. Our results compare well with experiment, especially the states involving a transition of the HC stretch (ν_1), and are generally within experimental error. Our results are generally much closer to the experimental values than are those of Jørgensen *et al.*, especially the fundamental bands

and transitions involving a change of ν_1. Our results are also closer to experiment than the results of Jakubetz and Lan.[27]

V. CONCLUSION

We have obtained new *ab initio* (semi)global potential energy and dipole moment surfaces for the HCN–HNC system, based principally on cc-pCVQZ CCSD(T) electronic structure calculations. The final calculated and fitted PES, termed VQZANO+, includes relativistic and adiabatic correction surfaces. Our best estimate for the critical energies on the VQZANO+ surface is that HNC lies 5281 cm^{-1} above the HCN absolute minimum. This value is reduced to 5186 cm^{-1} when zero-point energy effects are included. The barrier between these minima lies 16 798 cm^{-1} above the HCN

TABLE X. HCN band dipoles (Debye).

Transition	This work[a] [CCSD(T)]	CASSCF[b]	AQCC[c]	Expt.[d]
$(0,1^1,0) \rightarrow (0,0,0)$	0.1996(3)	0.27		0.189(1)
$(0,2^{2f},0) \rightarrow (0,1^1,0)$	0.1996(4)			0.188(4)
$(0,2^{2e},0) \rightarrow (0,1^1,0)$	0.1996(9)			0.189(4)
$(0,2^0,0) \rightarrow (0,0,0)$	0.0482(2)	0.048		0.0496(2)
$(0,0,1) \rightarrow (0,0,0)$	0.0018(4)	0.0	0.0012	0.001 362(4)
$(1,0,0) \rightarrow (0,1^1,0)$	0.0238(2)	0.02		0.0226(1)
$(0,1^1,1) \rightarrow (0,0,0)$	0.009 08(7)	0.012		0.008 24(5)
$(1,0,0) \rightarrow (0,0,0)$	0.0853(3)	0.095	0.070	0.0831(17)
$(1,1^1,0) \rightarrow (0,0,0)$	0.0098(2)	0.013		0.009 86(11)
$(1,0,1) \rightarrow (0,0,0)$	0.004 36(2)	0.0024	0.0024	0.0055

[a]Mean band dipole, with standard deviation given in last digit.
[b]*Ab initio* CASSCF and CCI calculations of Jørgensen *et al.* (Ref. 13), transformed from integrated band intensities to band dipoles.
[c]*Ab initio* TZP AQCC dipole surface calculations of Jakubetz and Lan (Ref. 27), transformed from integrated band intensities to band dipoles.
[d]Experimental data (Refs. 68 and 75–77).

TABLE XI. HNC fundamental band dipoles (Debye).

Transition	This work[a] [CCSD (T)]	AQCC[b]	Expt.[c]
$(0,1^1,0) \rightarrow (0,0,0)$	0.4627(5)		0.52(17)
$(0,0,1) \rightarrow (0,0,0)$	0.1035(3)	0.10	0.076(17)
$(1,0,0) \rightarrow (0,0,0)$	0.1509(4)	0.16	0.108(16)

[a]Mean band dipole, with standard deviation given in last digit.
[b]*Ab initio* TZP AQCC dipole surface of Jakubetz and Lan (Ref. 27), transformed from integrated band intensities to band dipoles.
[c]Experimental data (Ref. 78).

minimum. These last two values can be compared with 5126 ± 50 cm^{-1} and 16 733 cm^{-1}, obtained using a focal-point procedure. The focal-point estimates are expected to be more accurate than any others presently available.

In general our vibrational band origins are in good agreement with experiment. The main exception is the H–NC stretch for HNC with an anomalously large (20 cm^{-1}) error. We have morphed the HNC side of our potential with 17 aug-cc-pCVQZ CCSD(T) points, which cuts the error on our H–N(HNC) fundamental by a third. Therefore, a substantial part of the error in the original prediction of the H–N (HNC) fundamental appears to be caused by the cc-pCVQZ basis not being large enough to represent this part of the potential accurately.

We have calculated $J=0$ band origins for both HCN and HNC up to 12 400 cm^{-1} above the HCN zero-point energy, using our new surfaces. These band origins have been compared with the *ab initio* calculations of Bowman *et al.*[20] and with experimental data. The *ab initio* HCN vibrational band origins agree well with experiment and for the fundamental bands and C–H overtones are a significant improvement on the *ab initio* results of Bowman *et al.*[20] The *ab initio* HNC vibrational band origins also agree well with experiment and are a significant improvement over the results of Bowman *et al.* This improvement may well be due to the better representation of the HNC well by the cc-pCVQZ basis, and to improve further the surface it will be necessary to extend the size of the basis to beyond aug-cc-pCVQZ.

The geometries and energies of the HCN and HNC minima of our PES agree far better with experiment than does the Bowman *et al.* surface. The relativistic and adiabatic corrections have the effect of changing the relative energies of the HCN and HNC minima by 5.4 cm^{-1}, as is reflected in the change in the HNC(0,0,0) state relative to the HCN ZPE, between the VQZANO+ surface and the VQZANO2 surface, see Table VII. We have also calculated some representative pure rotational states ($J=1,5,10,15,20$) and some rovibrational states for the vibrational fundamentals ($J=1,5,10,15,20$) for both HCN and HNC. These states also agree well with experiment and demonstrate that the surface is useful for spectroscopic line assignments.

With our new potential and dipole surfaces we have calculated band transition dipoles for nine bands of HCN including the fundamentals and for the fundamental bands of HNC. We have compared these with experiment and found that they agree to within experimental error in all cases. These new surfaces are presently being used to generate an extensive, accurate, variational linelist for the HCN–HNC

system which will be used both to generate opacities for the atmospheres of cool stars and to aid the analysis of laboratory spectra of this system. Our best *ab initio* potential energy surface, VQZANO+, also provides an excellent starting point for determining a high accuracy surface using spectroscopic data for the combined HCN and HNC molecules. The surfaces due to Bowman *et al.*,[19,20] have been used as a starting point for a spectroscopically fitted surface,[21] which reproduce experimental vibrational band origins to within 1 cm^{-1}. As our experience has shown, a better starting point for a spectroscopic fit leads to a better fitted PES, so we would expect a significant improvement to the fitted HCN–HNC PES from our present starting point.

ACKNOWLEDGMENTS

[1] A. M. Smith, S. L. Coy, and W. Klemperer, J. Mol. Spectrosc. **134**, 134 (1989).
[2] D. Jonas, X. Yang, and A. Wodtke, J. Chem. Phys. **97**, 2284 (1992).
[3] D. Romanini and K. K. Lehmann, J. Chem. Phys. **102**, 633 (1995).
[4] A. Maki, W. Quapp, S. Klee, G. Ch. Mellau, and S. Albert, J. Mol. Spectrosc. **180**, 323 (1996).
[5] A. Maki, G. Ch. Mellau, S. Klee, M. Winnewisser, and W. Quapp, J. Mol. Spectrosc. **202**, 67 (2000).
[6] M. Lecoutre, F. Rohart, T. R. Huet, and A. G. Maki, J. Mol. Spectrosc. **203**, 158 (2000).
[7] K. K. Lehmann, private communication (2000).
[8] Z. Bačić and J. C. Light, J. Chem. Phys. **86**, 3065 (1987).
[9] M. Founargiotakis, S. C. Farantos, and J. Tennyson, J. Chem. Phys. **88**, 1598 (1988).
[10] V. Szalay, J. Chem. Phys. **92**, 3633 (1990).
[11] B. Leong Lan and J. M. Bowman, J. Phys. Chem. **97**, 12535 (1993).
[12] J. A Bentley, C. M. Huang, and R. E. Wyatt, J. Chem. Phys. **98**, 5207 (1993).
[13] U. G. Jørgensen, J. Almlöf, B. Gustafsson, M. Larsson, and P. Siegbahn, J. Chem. Phys. **83**, 3034 (1985).
[14] U. G. Jørgensen, Astron. Astrophys. **232**, 420 (1990).
[15] A. B. McCoy and E. L. Sibert III, J. Chem. Phys. **95**, 3476 (1991).
[16] S. Carter, I. M. Mills, and N. C. Handy, J. Chem. Phys. **97**, 1606 (1992).
[17] A. T. Wong and G. B. Bacskay, Mol. Phys. **79**, 819 (1993).
[18] S. Carter, N. C. Handy, and I. M. Mills, Philos. Trans. R. Soc. London, Ser. A **332**, 309 (1990).
[19] J. A. Bentley, J. M. Bowman, B. Gazdy, T. J. Lee, and C. E. Dateo, Chem. Phys. Lett. **198**, 563 (1992).
[20] J. M. Bowman, B. Gazdy, J. A. Bentley, T. J. Lee, and C. E. Dateo, J. Chem. Phys. **99**, 308 (1993).

[21] Q. Wu, J. Z. H. Zhang, and J. M. Bowman, J. Chem. Phys. **107**, 3602 (1997).

[22] T. J. Lee, C. E. Dateo, B. Gazdy, and J. M. Bowman, J. Chem. Phys. **97**, 8937 (1993).

[23] J. N. Murrell, S. Carter, and L. O. Halonen, J. Mol. Spectrosc. **93**, 307 (1982).

[24] J. F. Stanton and J. Gauss, J. Chem. Phys. **100**, 4695 (1994).

[25] A. M. Smith, U. G. Jørgensen, and K. K. Lehmann, J. Chem. Phys. **87**, 5649 (1987).

[26] A. M. Smith, W. Klemperer, and K. K. Lehmann, J. Chem. Phys. **90**, 4633 (1989).

[27] W. Jakubetz and B. Leong Lan, Chem. Phys. **217**, 375 (1997).

[28] A. G. Császár, W. D. Allen, Y. Yamaguchi, and H. F. Schaefer III, in *Computational Molecular Spectroscopy*, edited by P. Jensen and P. R. Bunker (Wiley, New York, 2000).

[29] MOLPRO 96 is a suite of *ab initio* programs written by H.-J. Werner and P. J. Knowles, with contributions by J. Almlöf, R. Amos, M. Deegan *et al.*

[30] NWCHEM, Version 3.3.1, High Performance Computational Chemistry Group, Pacific Northwest National Laboratory, Richland, Washington 99352, 1999.

[31] W. Kutzelnigg, Z. Phys. D: At., Mol. Clusters **11**, 15 (1989).

[32] W. Kutzelnigg, Phys. Rev. A **54**, 1183 (1996), and references therein.

[33] W. Klopper, J. Comput. Chem. **18**, 20 (1997).

[34] T. Helgaker, H. J. Aa. Jensen, P. Jørgensen *et al.*, DALTON 1.1.

[35] N. C. Handy, Y. Yamaguchi, and H. F. Schaefer III, J. Chem. Phys. **84**, 4481 (1986).

[36] C. L. Janssen, E. T. Seidl, G. E. Scuseria *et al.*, PSI 2.0.8, PSITECH Inc. (1995).

[37] K. Raghavachari, G. W. Trucks, J. A. Pople, and M. Head-Gordon, Chem. Phys. Lett. **157**, 479 (1989).

[38] T. J. Lee and P. R. Taylor, Int. J. Quantum Chem., Symp. **23**, 199 (1989).

[39] D. E. Woon and T. H. Dunning, Jr., J. Chem. Phys. **98**, 1358 (1993).

[40] T. H. Dunning, Jr., J. Chem. Phys. **90**, 1007 (1989).

[41] R. A. Kendall, T. H. Dunning, Jr., and R. J. Harrison, J. Chem. Phys. **96**, 6796 (1992).

[42] G. Winnewisser, A. G. Maki, and D. R. Johnson, J. Mol. Spectrosc. **39**, R149 (1971).

[43] R. C. Woods, Philos. Trans. R. Soc. London Ser. A **324**, 1578 (1988).

[44] R. A. Creswell and A. G. Robiette, Mol. Phys. **36**, 867 (1978).

[45] A. G. Császár and W. D. Allen, J. Chem. Phys. **104**, 2746 (1996).

[46] R. L. DeLeon and J. S. Muenter, J. Chem. Phys. **80**, 3892 (1984).

[47] P. Botschwinna, M. Horn, M. Matuschewski, E. Schick, and P. Sebald, THEOCHEM **400**, 119 (1997).

[48] G. L. Blackman, R. D. Brown, P. D. Godfrey, and H. I. Gunn, Nature (London) **261**, 395 (1976).

[49] D. Feller, J. Chem. Phys. **96**, 6104 (1992).

[50] A. G. Császár, G. Tarczay, M. L. Leininger, O. L. Polyansky, J. Tennyson, and W. D. Allen, in *Spectroscopy from Space*, edited by J. Demaison and K. Sarka, NATO ASI Series C (Kluwer, Dordrecht, 2001).

[51] T. van Mourik, A. K. Wilson, K. A. Peterson, D. E. Woon, and T. H. Dunning, Jr., Adv. Quantum Chem. **31**, 105 (1999).

[52] S. F. Boys and F. B. Bernardi, Mol. Phys. **19**, 553 (1970).

[53] A. K. Wilson, T. van Mourik, and T. H. Dunning, Jr., J. Mol. Struct.: THEOCHEM **388**, 339 (1996).

[54] T. van Mourik T. H. Dunning, Jr., and K. A. Peterson, J. Phys. Chem. A **104**, 2287 (2000).

[55] A. G. Császár, W. D. Allen, and H. F. Schaefer III, J. Chem. Phys. **108**, 9751 (1998).

[56] C. F. Pau and W. J. Hehre, J. Phys. Chem. **86**, 321 (1982).

[57] A. G. Maki and R. L. Sams, J. Phys. Chem. **75**, 4178 (1981).

[58] T. J. Lee and A. P. Rendell, Chem. Phys. Lett. **177**, 491 (1991).

[59] N. F. Zobov, O. L. Polyansky, C. R. Le Sueur, and J. Tennyson, Chem. Phys. Lett. **260**, 381 (1996).

[60] A. G. Császár, J. S. Kain, O. L. Polyansky, N. F. Zobov, and J. Tennyson, Chem. Phys. Lett. **293**, 317 (1998); **312**, 613 (1999).

[61] See EPAPS Document No. E-JCPSA6-114-307129 for electronic versions of lists of the *ab initio* data of 243 potential energy points, 242 dipole points, 242 relativistic correction points and 242 adiabatic correction points, FORTRAN routines and constants of the fits for the VQZANO+ PES, the dipole surface, the relativistic correction surface and the adiabatic correction surface. This document may be retrieved via the EPAPS homepage (http://www.aip.org/pubservs/epaps.html) or from ftp.aip.org in the directory epaps/. See the EPAPS homepage for more information.

[62] M. W. Chase *et al.*, J. Chem. Phys. Ref. Data **14**, 585 (1985).

[63] B. Gazdy and J. M. Bowman, J. Chem. Phys. **95**, 6309 (1991).

[64] M. Meuwly and J. M. Hutson, J. Chem. Phys. **110**, 8338 (1999).

[65] G. Brocks, J. Tennyson, and A. van der Avoird, J. Chem. Phys. **80**, 3223 (1984).

[66] J. Tennyson, J. R. Henderson, and N. G. Fulton, Comput. Phys. Commun. **86**, 175 (1995).

[67] H. Hönl and F. London, Z. Phys. **33**, 803 (1925).

[68] A. Maki, W. Quapp, and S. Klee, J. Mol. Spectrosc. **171**, 420 (1995).

[69] W. Gordy and R. L. Cook, *Microwave Molecular Spectra*, 3rd ed. (Wiley, New York, 1984).

[70] F. J. Northrup, G. A. Bethardy, and R. G. Macdonald, J. Mol. Spectrosc. **186**, 349 (1997).

[71] J. B. Burkolder, A. Sinha, P. D. Hammer, and C. J. Howard, J. Mol. Spectrosc. **126**, 72 (1987).

[72] F. Maiwald, F. Lewen, V. Ahrens *et al.*, J. Mol. Spectrosc. **202**, 166 (2000).

[73] L. S. Rothman, C. P. Rinsland, A. Goldman *et al.*, J. Quant. Spectrosc. Radiat. Transf. **60**, 665 (1998).

[74] T. Okabayashi and M. Tanimoto, J. Chem. Phys. **99**, 3268 (1987).

[75] A. Maki, W. Quapp, S. Klee, G. Ch. Mellau, and S. Albert, J. Mol. Spectrosc. **174**, 365 (1995).

[76] A. Maki, W. Quapp, S. Klee, G. Ch. Mellau, and S. Albert, J. Mol. Spectrosc. **185**, 356 (1997).

[77] J. Finzi, H. S. Wang, and F. Mastrup, J. Appl. Phys. **48**, 2681 (1977).

[78] M. Nezu, T. Amano, and K. Kawaguchi, J. Mol. Spectrosc. **192**, 41 (1998).